Karttunen, Anssi; von Hertzen, Raimo

A numerical study of traveling waves in a viscoelastic cylinder cover under rolling contact

Published in:
International Journal of Mechanical Sciences

DOI:
10.1016/j.ijmecsci.2012.11.006

Published: 01/01/2013

Document Version
Peer-reviewed accepted author manuscript, also known as Final accepted manuscript or Post-print

Please cite the original version:
Karttunen, A., & von Hertzen, R. (2013). A numerical study of traveling waves in a viscoelastic cylinder cover under rolling contact. *International Journal of Mechanical Sciences*, *66*, 180-191.
https://doi.org/10.1016/j.ijmecsci.2012.11.006

A numerical study of traveling waves in a viscoelastic cylinder cover under rolling contact

Anssi T. Karttunen[a,*], Raimo von Hertzen[a]

[a]*Department of Applied Mechanics, School of Engineering, Aalto University, P.O. Box 14300, FI-00076 Aalto, Finland*

Abstract

Polymer-covered cylinders are widely used in high-speed industrial rolling contact machines. In this paper, traveling waves which appear at high speeds in the viscoelastic polymer cover of a cylinder due to rolling contact are studied using a 2D finite element (FE) model for a two-cylinder system. Through eigenmode analysis of the polymer cover, it is found that an infinite number of natural mode families exist for the cylinder cover due to its finite thickness. A critical speed below which the traveling waves do not appear can be calculated on the basis of a resonance condition using the modal information. In dynamic analyses, traveling waves in the cover are identified as modified quasi-elastic Rayleigh waves composed of the eigenmodes of the polymer cover. The symbiosis of the eigenmode and wave propagation aspects allows the formation of a coherent overall picture of the traveling wave phenomenon. The critical speed according to the resonance condition is also the minimum phase velocity of the waves propagating in the cover. At the critical speed and above, there is a spectrum of resonant speeds due to wave dispersion. It is found that the traveling wave phenomenon is best described as a Rayleigh wave resonance in which contact-induced modified quasi-elastic Rayleigh waves arising at critical and supercritical speeds superpose to form a strong traveling shock wave.

Keywords: polymer cover, viscoelasticity, rolling contact, critical speed, Rayleigh wave resonance

1. Introduction

Over the past decades, the use of polymer-covered cylinders has become commonplace in high-speed industrial applications such as the calenders and size presses of paper machines. Nowadays, as a result of the increasing speeds of such industrial rolling contact machinery, dynamic physical phenomena which have been traditionally considered to be matters of minor importance are starting to play a pivotal role during machine operation and cause unforeseen problems. This creates a need for a thorough understanding of the dynamic behavior of high-speed rolling contact systems coated with viscoelastic polymers and sets new requirements for the design and development of industrial machines.

Many contact mechanical studies on viscoelastic cylinders focus on the analysis of contact stresses. The classical methods for elastic and inelastic bodies in rolling contact are well-established in the books by Johnson [1] and Kalker [2]. In recent years, the focus has been on applying advanced numerical techniques in rolling contact problems. For example, Gonzalez and Abascal have developed a novel boundary element formulation applicable to cylinders with viscoelastic coatings [3]. The formulations for contact stress analyses are often for rolling contact problems in which the inertial effects are not taken into account.

As for the dynamic behavior of viscoelastically covered rolling contact systems in general, two interconnected aspects are of key interest: the dynamic behavior of a viscoelastic cover itself and the vibrational behavior of an entire rolling contact system due to various sources of excitation. For example, the inherent

Recompiled, unedited accepted manuscript. Cite as: *Int. J. Mech. Sci.* 2013;66:180-191. doi link

*Corresponding author. Tel.: +358 (0) 405272713

Email addresses: anssi.karttunen@aalto.fi (Anssi T. Karttunen), raimo.von.hertzen@aalto.fi (Raimo von Hertzen)

self-excited vibration mechanism of polymer-covered rolling contact systems, in which viscoelastic deformations of the cover act as time-delayed feedbacks during rolling, is a problem which binds the cover behavior and the system vibrations together inseparably [4–7]. However, in the present study we concentrate on traveling waves in a viscoelastic cylinder cover that appear at high rolling speeds and can alone render industrial machines inoperable. These waves also contribute to the vibrational behavior of a rolling contact system, but the vibrations of an entire system are not considered in this paper.

The traveling waves studied in this paper are closely related to the widely studied standing waves in car tires, which emerge at high rolling velocities from the contact area between road and tire, and can be seen along the tire circumference. Actually, these standing waves are traveling waves in the tire, but appear to a non-rotating observer as stationary on the circumference of a rolling tire, as has been noted by many authors. In this paper, we use the term *tire standing waves* analogously to earlier studies dealing mainly with car tires as this terminology seems to be well-established.

A review on tire standing waves gathering the essential highlights of early studies was given by Ames [8]. A few years later, studies giving solid resonance-based physical interpretations on the phenomenon were made by Soedel [9] and Padovan [10, 11]. Modern treatises on viscoelastic structures in rolling contact using the finite element method and, also discussing tire standing waves, were first given by Oden and Lin [12], and Padovan et al. [13–15]. In their mathematical study of steady-state motions of a spinning cylinder, Rabier and Oden emphasized the close relationship between the standing waves in the cylinder and Rayleigh waves propagating in an elastic half-space [16]. In a recent paper, Krylov stated that the tire standing wave generation mechanism is the same as the one responsible, for example, for a sonic boom from a supersonic aircraft [17]. In the case of Krylov's vehicle tire model, the waves appear when the speed of the vehicle exceeds a certain critical speed of the tire flexural waves. Other approaches have also been used to characterise tire standing waves, for example, see [18–21]. The major outcome of most studies is the capability to predict a critical speed at which the waves first appear.

In this paper, we investigate the aforementioned traveling wave phenomenon in the case of a polymer-covered cylinder which is in rolling contact with a steel cylinder. The main objective of the present study is to establish, by understading the underlying physical mechanisms, a coherent overall picture of the traveling wave phenomenon. In order to achieve this goal, we develop a two-dimensional plane strain finite element (FE) model for the rolling contact system. The novelty of the model in comparison to thin shell, ring, tensioned beam, membrane etc. models is that the plane strain approach provides true insight into the polymer cover throughout its thickness. This enables us to combine the resonance and wave propagation interpretations known from the tire standing wave studies. The utilized industrial polymer is modeled as a linear isotropic viscoelastic material. The characteristics of the traveling waves in the polymer cover are investigated through eigenmode analysis of the cover and dynamic analyses of the system. The FE analysis is done using the FE software package Abaqus 6.10.

2. Methods

2.1. General setup

The two-cylinder rolling contact system under investigation consists of a steel cylinder having a radius of 0.4 m and a cylinder with a total radius of $R = 0.21$ m including a 6 mm thick viscoelastic polymer cover attached to a steel core (see Fig. 1). The dimensions of the system are those of an industrial rolling contact machine.

For the 2D computational model used in this work, the steel core of the polymer-covered cylinder is modeled as rigid and the polymer as a linear isotropic viscoelastic material. The steel cylinder is modeled as a rigid surface. The contact between the cylinders is frictionless. In a reference frame fixed to the viscoelastically covered cylinder, the other cylinder moves in rolling contact around the covered cylinder which in this frame appears to be at rest. The FE model is developed in this frame of reference since it saves a lot of computation time and the constraints of the bottom, that is, the inner surface of the polymer cover, are better fulfilled in the numerical calculations. In the model, the rolling contact between the cylinders is realized by a massless connector rod which is attached to the centerpoints of the cylinders and may be given,

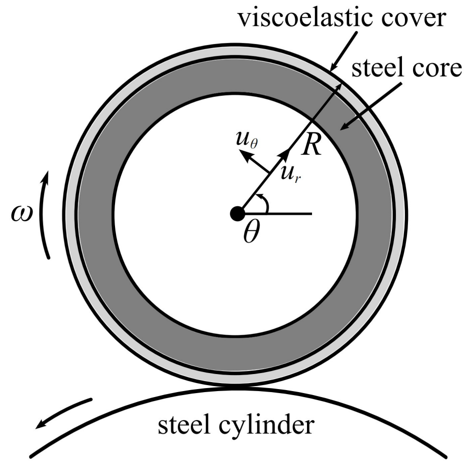

Figure 1: Two-dimensional rolling contact system with a viscoelastic polymer cover on the other cylinder.

as time-dependent kinematic conditions, an angular velocity ω and an axial force or contraction, to form the contact between the cylinders, otherwise the rod is rigid. In section 3.4, the same constant contraction is given for the rod in all rolling contact analyses. Fig. 2 shows a detail of the meshed polymer cover with an element size of 0.3 mm. Linear isoparametric quadrilateral plane strain elements are used with unit thickness[2].

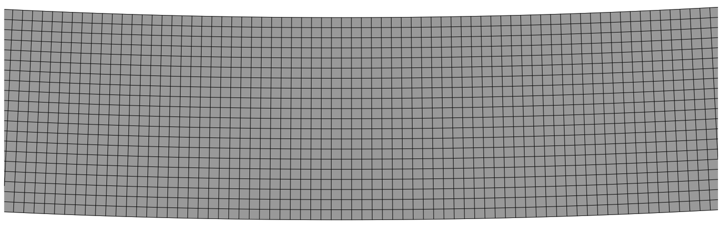

Figure 2: Mesh detail of the polymer cover. The element size, that is, the length of each side of a quadrilateral element, is approximately 0.3 mm.

Because the polymer-covered cylinder is modeled as stationary, the Coriolis and centrifugal forces acting on the polymer cover in an actual industrial machine due to rotation are not intrinsically accounted for. The effects of these forces on the system are studied and discussed in connection with the eigenmode and dynamic analyses in sections 2.3 and 3.4, respectively.

2.2. Constitutive behavior of the viscoelastic polymer cover

Within the context of small strains, the constitutive equation for an isotropic viscoelastic material can be written in a hereditary integral form as

$$\boldsymbol{\sigma}(t) = \int_0^t 2G(t-\tau)\frac{d\mathbf{e}}{d\tau}(\tau)d\tau + \mathbf{I}\int_0^t K(t-\tau)\frac{d\phi}{d\tau}(\tau)d\tau \ , \tag{1}$$

where $\boldsymbol{\sigma}$ is the Cauchy stress tensor, G is the shear modulus, K is the bulk modulus, $\mathbf{e}$ is the deviatoric part of the strain, ϕ is the volumetric part of the strain, t is current time, τ is past time and $\mathbf{I}$ is the identity tensor [22].

[2]Abaqus elements CPE4H (eigenmode analysis) and CPE4R (explicit dynamic analysis)

The moduli in Eq. (1) can be represented in terms of the Prony series which corresponds to a generalization of the classical Maxwell model of viscoelasticity, which in 1D consists of a spring and Maxwell elements assembled in parallel. For the shear modulus we get

$$G(t) = G_0 \left[1 - \sum_{i=1}^{N} g_i (1 - e^{-t/\tau_i^G}) \right] , \tag{2}$$

where $g_i = G_i/G_0$ and the instantaneous shear modulus is $G_0 = G_\infty + \sum G_i$ [22]. The material parameters G_i, G_∞ and τ_i^G are obtained from test data. An expression analogous to Eq. (2) can be written for the bulk modulus. However, for polymeric materials the bulk response is often practically elastic and much stiffer than the deviatoric response due to nearly incompressible behavior [23, 24]. This is also the case for the viscoelastic polymer utilized in this study; thus, we model the volumetric behavior of the polymer to be elastic. The material parameters used are given in Table 1. To perform the numerical analysis, Eq. (1) needs to be incorporated into the numerical solution of the model, see [22, 23].

Table 1: Viscoelastic material parameters of the polymer cover obtained from Dynamic Mechanical Thermal Analysis (DMTA). The instantaneous Young's modulus is $E_0 = 17.58$ MPa, the Poisson's ratio $\nu = 0.49$, and $G_0 = \frac{1}{2}E_0/(1+\nu) = 5.9$ MPa. The density of the polymer is $\rho = 2000$ kg/m^3.

i	1	2	3	4	5	6	7
g_i	0.1496	0.0935	0.0705	0.0486	0.0436	0.0413	0.0347
τ_i^G[s]	10^{-4}	10^{-3}	10^{-2}	10^{-1}	10^{0}	10^{1}	10^{2}

The material parameters span a sufficiently wide relaxation spectrum to model the mechanical behavior of the polymer realistically. In this study, viscoelastic relaxation processes related to the time scales of 10^3 and 10^{-5} s and beyond are assumed to be inactive considering the maximum duration of the dynamic simulations and the contact dwell times.

2.3. Eigenmode analysis

The natural frequencies and mode shapes of the cover layer of the polymer-coated cylinder are computed using the shifted block Lanczos method [25]. In the computations, the frequency-dependent behavior of the viscoelastic polymer is taken into account. Thus, the elastic properties of the polymer need to be evaluated at a chosen ("dependent") frequency before performing the eigenmode analysis. In short, if a block of material is excited by a harmonic force, the material stiffness properties need to be computed so that they correspond to the frequency of the force.

In this study, the material properties of the polymer cover for the eigenmode analysis are determined according to the resonance condition, that is to say, the dependent frequency to determine the material parameters is matched with the computed natural frequency by iteration for each mode. This is greatly facilitated by the Lanczos method that allows one to perform each eigenmode analysis in a small frequency range as the dependent frequency is increased gradually in the successive calculation of the eigenmodes. The contact itself between the cylinders is not considered in the computations because the contact area, the nip, is relatively small and localized having a negligible effect on the natural frequencies and modes of the polymer cover.

To illustrate a typical mode shape, a computed natural mode of the polymer cover is shown in Fig. 3. It is characteristic for the modes to have a certain number of waves on the cylinder circumference. In this case, the number of waves is one hundred, that is, the principal mode number for the shown mode is $N = 100$. The corresponding natural frequency is $f_{100} = 5016$ Hz. Modes consisting of sine-like waves on the cylinder circumference, as shown in Fig. 3, are called the primary modes hereafter (see also Fig. 6).

Fig. 4 shows the relative differences between the natural frequencies of the primary modes for different element sizes as a function of the principal mode number N. The smallest element size, 0.15 mm, has been

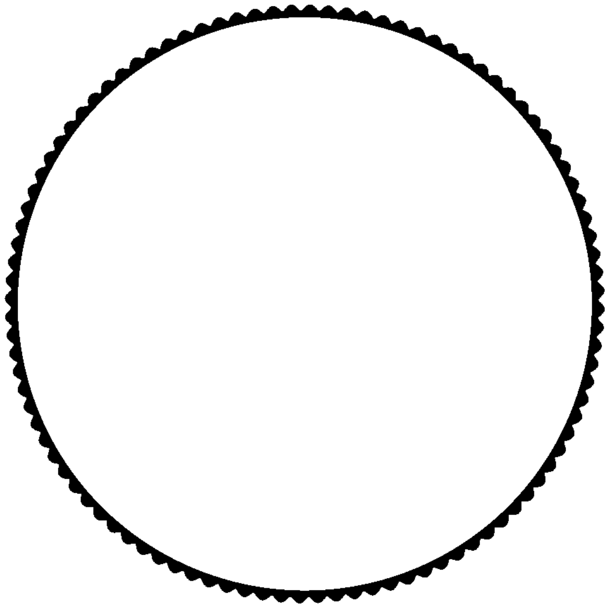

Figure 3: Computed eigenmode of the polymer cover for which the principal mode number, that is, the number of full waves on the cylinder circumference, is $N = 100$. The corresponding natural frequency is $f_{100} = 5016$ Hz.

chosen as the reference. As the mode number increases, the relative differences increase. The more waves there are on the cylinder circumference, the more elements are needed to depict the modes correctly. The differences between the two smallest element sizes are comparatively small ($< 1\%$). It can be estimated that if the smallest element size would be halved, the increase in accuracy would be fairly low. In all eigenmode calculations and dynamic simulations, the element size 0.3 mm is used and the model consists of 86680 elements.

The modeled polymer-covered cylinder does not rotate, but the centrifugal force can be added as a rotational body force to the model to study how it affects the natural frequencies and modes. A rotational frequency for the cylinder to study the effect of the centrifugal force on the modes is computed following the physical interpretation given by Soedel for the tire standing wave phenomenon [9]. In the case of our model, in dynamic rolling contact analyses the contact forces act as a disturbance traveling around the cylinder with a rotational speed ω. If the disturbance travels over one full wave of an eigenmode, with the wavelength λ_N on the cylinder cover, in the same time it takes for the eigenmode to go through one oscillation, that eigenmode will go into resonance. The time to travel over one wavelength is

$$T = \frac{\lambda_N}{\omega R} = \frac{2\pi}{N\omega} = \frac{1}{Nf} \; , \tag{3}$$

where $f = \omega/2\pi$ is the rotational frequency of the disturbance. On the other hand, the period of oscillation of the mode is

$$T = \frac{2\pi}{\omega_N} = \frac{1}{f_N} \; . \tag{4}$$

From Eqs. (3) and (4), we get the resonance condition

$$\omega = \frac{\omega_N}{N} \; , \tag{5}$$

or

$$f = \frac{f_N}{N} \; . \tag{6}$$

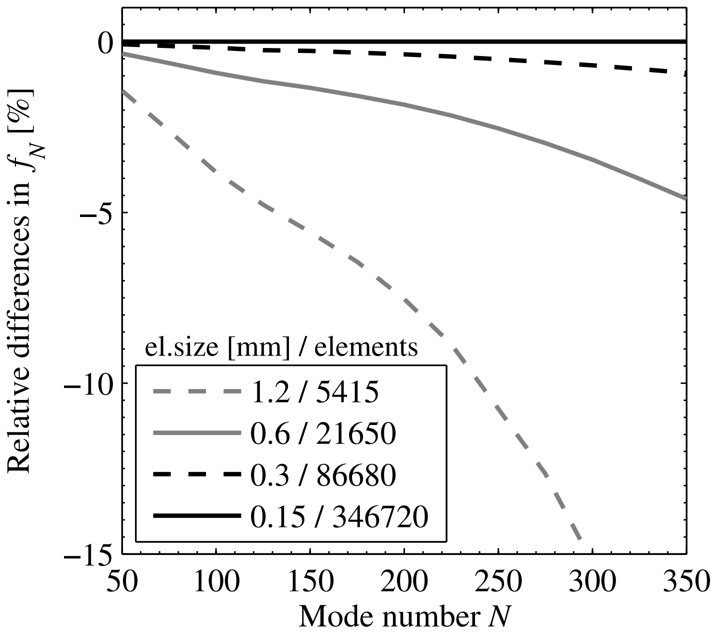

Figure 4: Relative differences between computed natural frequencies of the primary modes defined as $(f_{N,el.size} - f_{N,0.15})/f_{N,0.15} \times 100$ for different element sizes as a function of the principal mode number N. The relative difference between the two smallest element sizes for $N = 100$ is 0.18 %, for example.

The rotational frequency for the cylinder to assess the significance of the centrifugal force is computed according to Eq. (6), since, as it will be seen later, this equation is closely related to the critical speed of the traveling wave phenomenon studied in this paper. Again, the material's dependent frequency is matched with the computed natural frequency by iteration. It is found that the centrifugal force does not change the shapes of the modes notably, but its effect is best seen in Table 2 which shows the contribution of the centrifugal force to the natural frequencies of the system. The force causes a small decrease in the natural frequencies that is more intense at lower modes, that is, at high rotational speeds, which are of secondary interest in the study of the emergence of traveling waves in the polymer cover. A decrease in the natural frequencies due to centrifugal force also occurs in the case of a rotating disk [26]. In the case of a ring model, on the other hand, the natural frequencies increase with an increasing speed [27]. In this regard, the studied model conforms better to the rotating disk than the ring model. In general, at low ratios of f/f_N, as is the case for the studied model, the effect of the centrifugal force on the natural frequencies is small [26, 27]. The same also holds for the Coriolis force as its effect on the natural frequencies is typically of the same order as that of the centrifugal force [26, 27]. Since the Coriolis and centrifugal forces have little effect on the eigenmodes, these forces are not accounted for in the eigenmode analysis in this study.

Table 2: Effect of the centrifugal force on the natural frequencies f_N of the polymer cover at rotational frequency f_{cen} according to Eq. (6). In Eq. (6), the corrected value $f_{N,cen}$ is used. The relative difference between $f_{N,cen}$ and f_N is given by $(f_{N,cen} - f_N)/f_N \times 100$.

N	f_{cen} [Hz]	$f_{N,cen}$ [Hz]	f_N [Hz]	Rel. diff. [%]
50	79.82	3991	4025	-0.84
75	60.87	4565	4587	-0.48
200	40.17	8034	8039	-0.06

2.4. Contact modeling

To model the frictionless contact between the cylinders, a penalty contact algorithm is used to enforce the contact constraints. The algorithm searches for penetrations of the slave nodes on the polymer cover into the rigid master surface in the current configuration. Then, forces that are a function of the penetration distance are applied according to the utilized pressure-overclosure relationship to the slave nodes to oppose the penetration, while equal and opposite forces act on the rigid surface at the penetration point.

For the following equations in this section, see [22]. Let us define a contact pressure p between two surfaces at a point as a function of the overclosure h, that is, the interpenetration of the surfaces at that point. Now, a contact pressure-overclosure relationship for a "hard" contact is

$$p = 0 \quad \text{for} \quad h < 0 \quad \text{(open)} \tag{7}$$

$$h = 0 \quad \text{for} \quad p > 0 \quad \text{(closed)} \; . \tag{8}$$

For a "softened" contact with an exponential pressure-overclosure relationship two additional parameters are defined: an initial contact distance c and a typical pressure value p_0, which is the pressure value at zero overclosure $h = 0$. For the softened contact, the p-h relationship is

$$p = 0 \quad \text{for} \quad h \leq -c \tag{9}$$

$$p = \frac{p_0}{(e-1)} \left[\left(\frac{h}{c} + 1 \right) \left(e^{h/c+1} - 1 \right) \right] \quad \text{for} \quad h > -c \; . \tag{10}$$

The hard contact relationship leads to noisy solutions, mainly because of the strong hourglassing of the quadrilateral elements using reduced integration in explicit dynamic analysis. To overcome the hourglassing, the softened contact is used instead. Fig. 5 shows the contact pressure for the hard and softened contacts in a non-rotating case. An axial force has been given for the connector rod, and for the softened contact the initial contact distance parameter has been set to $c = 0.05$ mm and the pressure parameter to $p_0 = 0.1$ MPa. The same parameter values are used for all rolling contact analyses in section 3.4. The contact area for the softened contact is wider and the peak value for the contact pressure is lower. The softening removes drastic changes in contact forces between neighboring nodes at the contact edges. This reduces the hourglassing of the elements together with the physical stabilization method used that utilizes a combination of artificial stiffness and damping to control the hourglass modes [22, 28].

The softened contact approach provides essential computational benefits, although it is only an approximation of the real contact conditions that may be closer to the ones provided by the hard contact. However, let us note that according to Padovan, the critical speed at which the traveling wave phenomenon takes place is independent of the distributional nature of the traveling surface tractions [10], which also implies that friction has no effect on the onset of the traveling wave phenomenon. Moreover, according to Kennedy and Padovan [15], if friction is included into a tire contact model, it causes very localized shear distributions in the contact area, but hardly affects the global dynamic response of the system. Often simple point loads have been used to generate the tire standing wave effects, for example, see [9, 17]. The role of the loading is mainly to act as a supply of energy required to propagate and sustain a wave.

2.5. Explicit dynamic analysis and computational details

The dynamic simulations are performed by using Abaqus/Explicit. To calculate the response of a system, Abaqus utilizes explicit central-difference based time integration. For a comprehensive treatment of the explicit time integration procedure, see [29]. Considering an increment during simulation, the general procedure for the computations can be presented in a concise form as follows (see [22]). Accelerations are computed by

$$\ddot{u}_{(i)} = M^{-1} \left(F_{(i)} - I_{(i)} \right) \; , \tag{11}$$

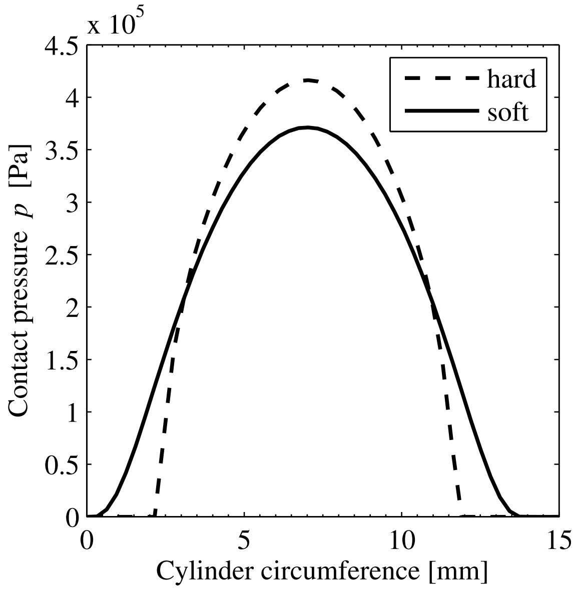

Figure 5: Contact pressures for the hard and softened contacts in a non-rotating case. The areas under the curves, that is, the resultant forces, are equal.

where u contains the nodal degrees of freedom of the elements, M is the diagonal mass matrix, F is the vector of applied forces, I is the vector of internal forces and index i refers to temporal development. Velocities and displacements are computed by

$$\dot{u}_{(i+1/2)} = \dot{u}_{(i-1/2)} + \frac{\Delta t_{(i+1)} + \Delta t_{(i)}}{2} \ddot{u}_{(i)} \tag{12}$$

$$u_{(i+1)} = u_{(i)} + \Delta t_{(i+1)} \dot{u}_{(i+1/2)} \ . \tag{13}$$

After this, the element level calculations are performed and then the next incremental step is taken.

In the explicit method, each increment is computationally inexpensive, because there are no simultaneous equations to be solved. An approximation for the stable time increment is

$$\Delta t_{stable} \approx \frac{L_{min}}{c_d} \ , \tag{14}$$

where L_{min} is the smallest element dimension in the mesh and the dilatational wave speed is

$$c_d = \sqrt{\frac{\hat{\lambda} + 2\hat{\mu}}{\rho}} \ , \tag{15}$$

where $\hat{\lambda}$ and $\hat{\mu}$ are the effective Lame constants, and ρ is the density of the material. With a dense mesh, Eq. (14) typically results in very small time increments. Therefore, the explicit method is naturally suitable for achieving high resolution solutions for high-speed transient dynamic events and, especially, if contact conditions need to be updated within small time intervals.

The studied FE model can be decomposed efficiently into eight domains, which allows the use of parallel computing. The memory requirements in the explicit method are very low, due to the absence of a global stiffness matrix required in implicit methods in particular.

By default, Abaqus uses artificial bulk viscosity damping to introduce some damping into an explicit model and contact damping in association with the penalty contact algorithm. However, in this study these sources of dissipation have been removed because the viscoelasticity of the polymer cover provides sufficient damping.

3. Results and discussion

3.1. Natural frequencies and modes

Fig. 6 shows close-up views of three different mode families of the polymer cover. The dark color stands for positive and white for negative radial displacements. In each mode family, every individual mode possesses an integer number of waves on the cylinder circumference. For all the shown modes the number of waves is one hundred, thus the principal mode number in all cases is $N = 100$. The sine wave-type primary mode in Fig. 6a was shown in full in Fig. 3. Secondary mode families I and II are presented in Figs. 6b and 6c, respectively. For the modes in Figs. 6a–c, the corresponding natural frequencies are 5016, 8296 and 11838 Hz, respectively.

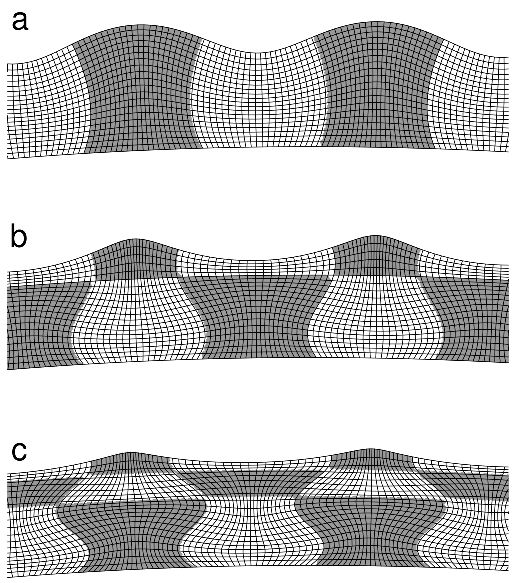

Figure 6: Three mode families. The principal mode number in all cases is $N = 100$. The dark and white areas represent positive and negative radial displacements, respectively. a) Primary mode, $f_{100} = 5016$ Hz, b) Secondary mode I, $f_{100} = 8296$ Hz, c) Secondary mode II, $f_{100} = 11838$ Hz.

The distinction between the different mode families can be made clear by looking at the radial displacements. For the primary mode in Fig. 6a the radial displacement does not change sign along an initially straight radial line from the bottom to the surface of the polymer cover. For the secondary modes in Figs. 6b and 6c, the sign changes once and twice, respectively, in the radial direction.

More than the three shown mode families exist for the polymer cover. In fact, due to the finite thickness of the cover layer, there are an infinite number of higher mode families, each of which corresponds to a secondary mode number. Due to the thinness of the cover layer the higher mode families appear at very high frequencies and are of minor interest in the development of traveling waves due to rolling contact. They would also require a larger number of finite elements to be used to depict the modes correctly due to an increasing number of sign changes in both radial and tangential displacements leading to more complex shapes. It can also be seen that the more sign changes there are in the displacements, the flatter the modes tend to appear. Consequently, the waves on the cylinder circumference become increasingly lower and sharper for the higher mode families.

Fig. 7 shows the radial and tangential displacements of the surface nodes along the circumference of the polymer cover for the primary mode presented in Fig. 6a. The radial displacement precedes the tangential one by a phase shift of 90 degrees. Contrary to the surface, on the midsurface of the polymer cover, that is, 3 mm beneath the cover surface, the tangential displacement precedes the radial one by 90 degrees. The phase change between the surface and the midsurface is not continuous; instead, a sudden change of 180

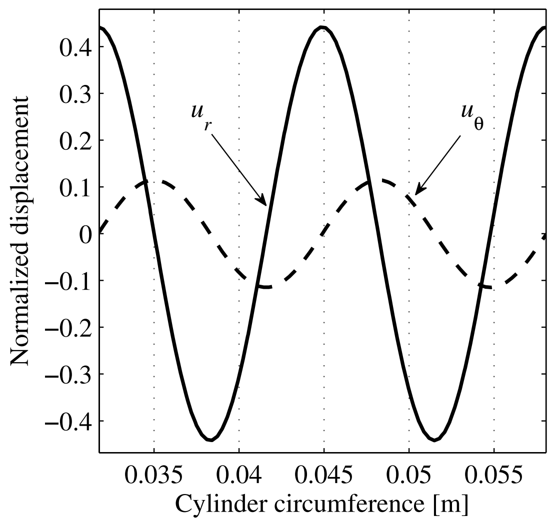

Figure 7: Radial and tangential displacements of the surface nodes of the polymer cover for the primary mode $N = 100$. The radial displacement precedes the tangential one by 90 degrees.

degrees occurs between the third and fourth node beneath the surface. Further changes do not take place for the primary modes. Similar phase changes also occur for the secondary mode families. These results are consistent with the well-known fact that for axisymmetric systems the phase difference between the radial and tangential displacements of the eigenmodes is ±90 degrees [9, 30].

The natural frequencies of each mode family of Fig. 6 as a function of the principal mode number N are shown in Fig. 8. Due to the vicinity of the discrete points, the curves are plotted as continuous lines. The lowest primary mode appears at 2200 Hz and the lowest secondary modes I and II at 6700 Hz and 11200 Hz, respectively. The natural frequencies of each mode family increase steadily for increasing mode number with the small exceptions for the secondary modes I and II, which experience slight decreases from the lowest modes up till $N = 40$ and $N = 25$, respectively. At higher mode numbers, the illustrated curves display almost constant slopes.

3.2. Traveling waves due to harmonic load

In one dimension, two interfering identical waves traveling in opposite directions with the same phase velocity produce a standing wave. Let us study such traveling waves with the current 2D model. A harmonic load with the frequency 5016 Hz corresponding to the natural frequency f_{100} of the primary mode is exerted on five adjacent surface nodes on the cover. A modified Rayleigh wave, which is generated by the load and propagates along the circumference of the polymer cover, is shown in Fig. 9. An identical wave travels in the opposite direction. The calculated wavelength $\lambda = 0.0132$ m is equal to one hundredth of the outer circumference of the polymer cover and, thus, equals the wavelength λ_{100} of the primary natural mode. It is evident that if the two waves generated by the harmonic load and traveling in opposite directions interfere on the other side of the cover, they form a standing wave similar to the primary eigenmode corresponding to $N = 100$ which then spreads over the whole circumference creating a resonance response. This is demonstrated in a purely elastic case for the primary mode $N = 50$ in Fig. 10.

In Fig. 10, the radial displacement of the cover surface for half of the cylinder circumference is shown at moments t_0 (black) and $t_0 + T_{50}/2$ (grey) when the primary mode $N = 50$ is excited by a same type of harmonic load as in Fig. 9. The traveling waves interfere and a standing wave starts to form, and shortly after it dominates around the circumference as can be seen in Fig. 10. The vibration amplitudes increase steadily due to the lack of dissipation indicating a resonance response. The situation here is analogous to, for example, the higher-order spheroidal free oscillations of Earth which are equivalent to the standing

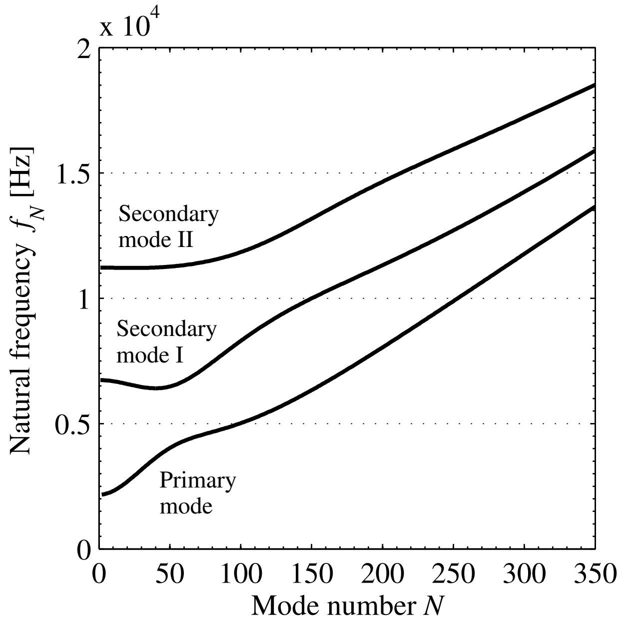

Figure 8: Natural frequencies for the primary modes and secondary modes I and II of the polymer cover as a function of the principal mode number N.

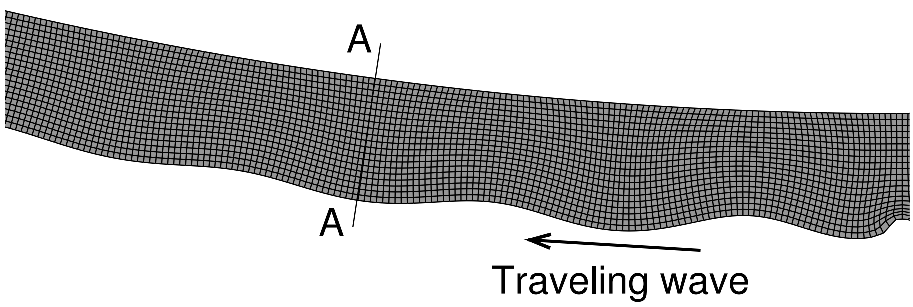

Figure 9: Traveling wave in the viscoelastic cylinder cover in steady-state. A harmonic load is exerted on five surface nodes. The center node (rightmost in the figure) and its adjacent nodes on both sides are loaded with a vertical harmonic point load of 200 N. For the nodes next to the adjacent nodes the load magnitude is 100 N. The displacements have been upscaled for illustrative purposes. Due to the finite depth of the polymer layer, the wave is classified as a modified Rayleigh wave according to [31]. Due to symmetry only the left part of the cover is shown.

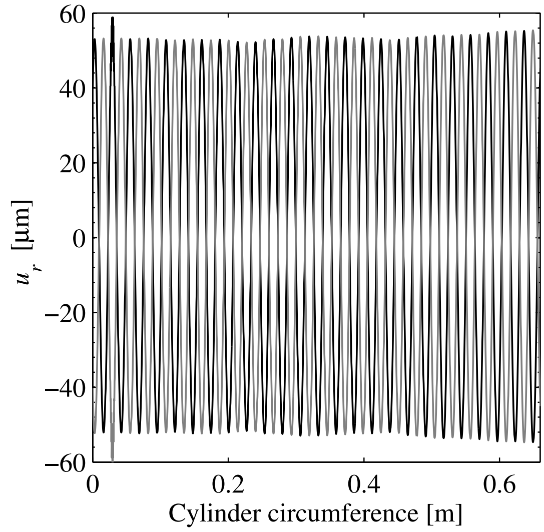

Figure 10: Radial displacement of the cover surface for half of the cylinder circumference at moments t_0 (black) and $t_0 + T_{50}/2$ (grey) for a harmonic load with the frequency 4067 Hz which equals the primary natural frequency f_{50} of an elastic cylinder cover. The cover drifts into a state of vibration dominated by the standing wave resonance oscillations corresponding to the primary eigenmode $N = 50$. The two higher peaks are caused by the loading. A small amount of artificial damping was used for numerical stability in the elastic case.

wave patterns that arise from the interference of trains of long-period Rayleigh waves traveling in opposite directions around the Earth [32]. Note also that the excitation frequency of 4067 Hz is well below the cutoff frequencies, 6435 and 11223 Hz, of the secondary Rayleigh waves corresponding to the lowest secondary modes I and II in the purely elastic case, respectively. The only traveling waves leading to a standing wave correspond to the primary mode. This can be clearly seen in Fig. 11 which shows corresponding portions of the elastic primary eigenmode $N = 50$ of the polymer cover and the harmonically excited cover of Fig. 10. The displacements corresponding to the secondary modes are exponentially decayed and appear only locally in the immediate vicinity of the applied load. The behavior of the cylinder cover is, however, quite different if there is enough dissipation in the viscoelastic cover. For the viscoelastic parameter values of the present work, for example, the radiated traveling waves attenuate fast when the primary mode $N = 100$ is excited, as shown in Fig. 12, and the waves never interfere. Thus, no standing wave vibration forms.

The displacements of the element nodes along the cross-section A-A in Fig. 9 are investigated in Fig. 13. Displacement paths for the three nodes closest to the surface of the cover are presented in Fig. 13a. The nodes experience an elliptic retrograde motion in which the radial displacement precedes the tangential one by 90 degrees. The major axes of the ellipses are almost vertical. The motion changes sense between the nodes 3 and 4 from retrograde to prograde, and a phase change of 180 degrees takes place between the radial and tangential displacements, which is in accordance with the similar phase change for the primary mode $N = 100$ explained earlier. No further changes take place. Note that similar behavior is characteristic to quasi-elastic Rayleigh waves over a half-space of viscoelastic material for which the major axes of the elliptic particle paths are vertical and the motion is retrograde on the surface and changes sense once below the surface [33]. Therefore, we further classify the traveling wave of Fig. 9 as a modified quasi-elastic Rayleigh wave. In Fig. 13b, the vibration amplitudes of each node in both radial and tangential directions along the cross-section A-A of Fig. 9 are shown. The radial amplitude reaches its maximum at node 3, after which it exhibits a steady decrease. The tangential amplitude is small at the sense change, as expected, but starts to increase to reach its maximum at node 13. At node 12 the amplitudes are almost equal and the displacement path is of a circular type. After this, the tangential displacements dominate towards the bottom. The motion of node 21 at the bottom of the polymer cover is prevented by the boundary conditions.

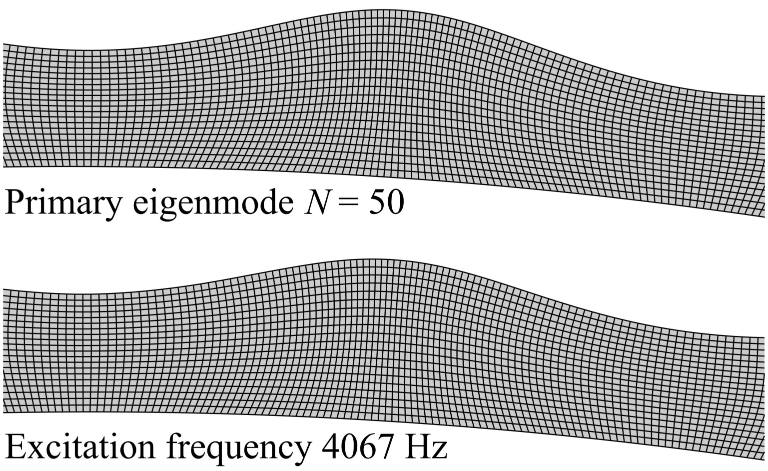

Figure 11: The elastic primary eigenmode $N = 50$ and the harmonic loading case of Fig. 10. The excitation frequency 4067 Hz is below the cutoff frequencies 6435 and 11223 Hz of the secondary mode families I and II, respectively. Therefore, the calculated standing wave due to the harmonic load is practically identical to the primary mode $N = 50$.

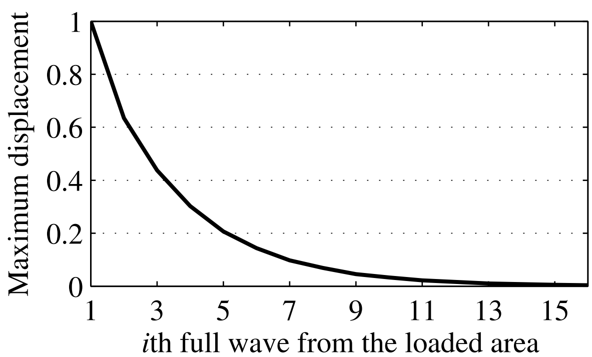

Figure 12: Attenuation of the traveling waves of Fig. 9. Vertical axis shows the relative maximum displacement of the top of a full wave with the wavelength $\lambda = 0.0132$ m. The displacement drops to practically zero around the 16th wave from the loading. Thus, the traveling waves propagating in both directions from the loading cover altogether approximately one third of the cylinder circumference as the primary mode $N = 100$ is excited.

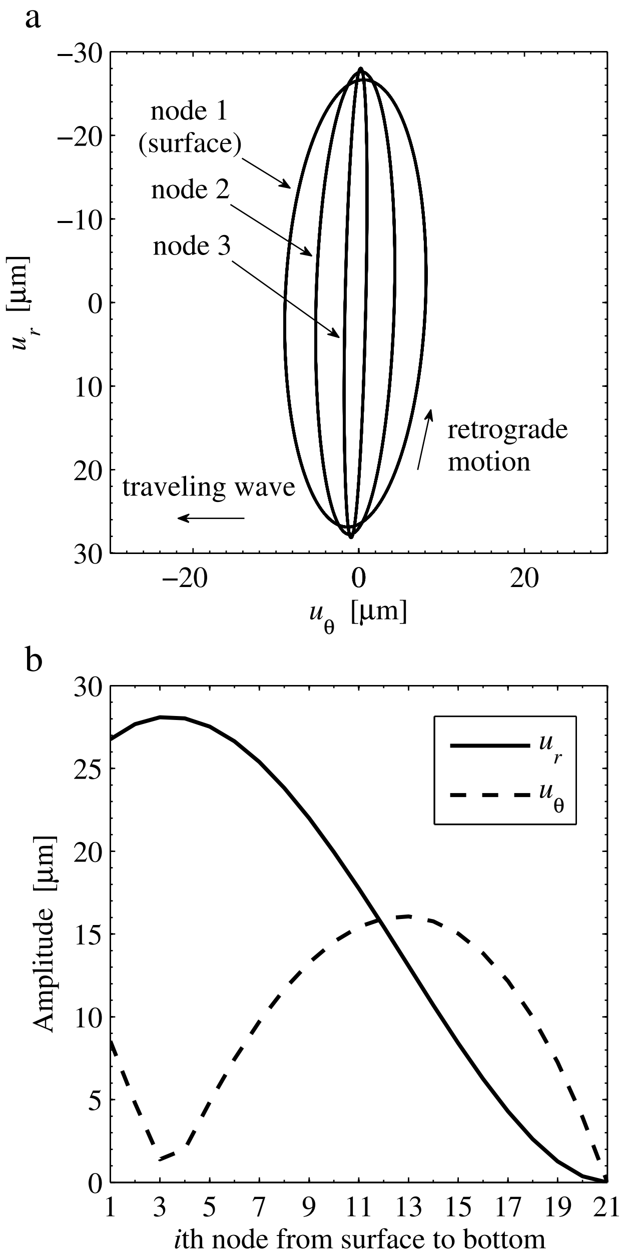

Figure 13: a) Displacement paths for the three nodes closest to the cover surface along the cross-section A-A in Fig. 9 during 25 consecutive vibration periods. b) Radial and tangential vibration amplitudes for the nodes along the cross-section A-A. The elliptic motion changes sense between the nodes 3 and 4 from retrograde to prograde.

3.3. *Physical interpretation and critical speed*

Let us consider a modified Rayleigh wave with a wavelength of $2\pi R/N$. As was pointed out in the previous section, the frequency of this wave equals the natural frequency f_N of the Nth eigenmode. Therefore, the phase velocity of this Rayleigh wave is

$$v_p = \frac{2\pi R}{N} f_N = 2\pi R \frac{f_N}{N} \ , \tag{16}$$

or equivalently

$$\frac{v_p}{2\pi R} = \frac{f_N}{N} = f \ , \tag{17}$$

where f, according to Eq. (6), is the rotational frequency of the contact load which resonates with the Nth eigenmode of the cover. The computed values of f_N/N as a function of the natural frequency f_N and as a function of the principal mode number N are presented for each mode family in Figs. 14 and 15, respectively. In both figures the curves of the primary modes approach a constant value around 39 Hz at higher modes, indicating that there is a cutoff rotational frequency, or a critical speed (51.5 m/s), under which the resonance condition is not fulfilled by any mode.

Considering, on the other hand, the wave propagation, one can see that also the phase velocity of the modified quasi-elastic Rayleigh waves approaches a constant value at higher frequencies. This means that the high frequency waves in the cover layer become non-dispersive, as is the case for Rayleigh waves over an elastic half-space. The phase velocity of the Rayleigh waves in an elastic half-space is given by the approximate formula [34]

$$c_R = \frac{0.87 + 1.12\nu}{1+\nu} \sqrt{\frac{G}{\rho}}. \tag{18}$$

Using the values $G = G_0 = 5.9$ MPa, $\nu = 0.49$ and $\rho = 2000$ kg/m^3 from Table 1, Eq. (18) gives $c_R = 51.7$ m/s, which is very close to the critical speed 51.5 m/s in Fig. 15.

It is well-known that the characteristic penetration depth of a Rayleigh wave is approximately one-half of its wavelength [32]. In other words, when the wavelength is less than twice the thickness of the cover layer, the finite thickness of the layer hardly affects the wave behavior. This is also evident in Fig. 15. For example, for the mode number $N = 110$ the wavelength is 12 mm which is twice the layer thickness and, as can be seen in Fig. 15, the corresponding phase velocity of the primary wave is relatively near the asymptotic value. For smaller mode numbers, that is, for larger wavelengths, the bottom of the layer starts to affect the wave propagation and, consequently, the phase velocity increases, bringing about dispersion as well. For the secondary Rayleigh waves, corresponding to the secondary eigenmodes, the effect of the bottom is more significant than for the primary waves.

Considering the eigenmode-based resonance approach in conjunction with the eigenmode expansion of the modified Rayleigh wave leads one to the intriguing conclusion that the traveling waves cannot exist in the subcritical region because all the natural modes in the eigenmode expansion of the wave are subcritically excited. Thus, the modes have small phase lags with respect to the load leading to a quasistatic, that is, local and non-propagating disturbance. The foregoing implies that the critical speed is also the minimum phase velocity of the modified Rayleigh waves in the polymer cover. Thus, a different approach to be taken with the traveling wave problem would be to determine the dispersion relation for the traveling waves to get the critical speed. For circular cylinders and car tires one way to achieve this within the framework of the finite element method is to use the waveguide FEM. For a formulation of the method for curved structures, including linear viscoelasticity, see [35]. The waveguide finite elements have been successfully applied, for example, to study the sound radiation of a rolling tire [36], an acoustical problem closely related to the mechanical one of this study from the wave dispersion perspective.

The wave propagation aspect is particularly interesting since it is known in the case of an elastic ring that when the load velocity is below the minimum phase velocity of the waves in the ring, the resulting deformation pattern remains localized – whereas a resonance occurs and the load starts to radiate traveling waves when the velocity of the load exceeds the minimum phase velocity of the waves in the ring [37]. We

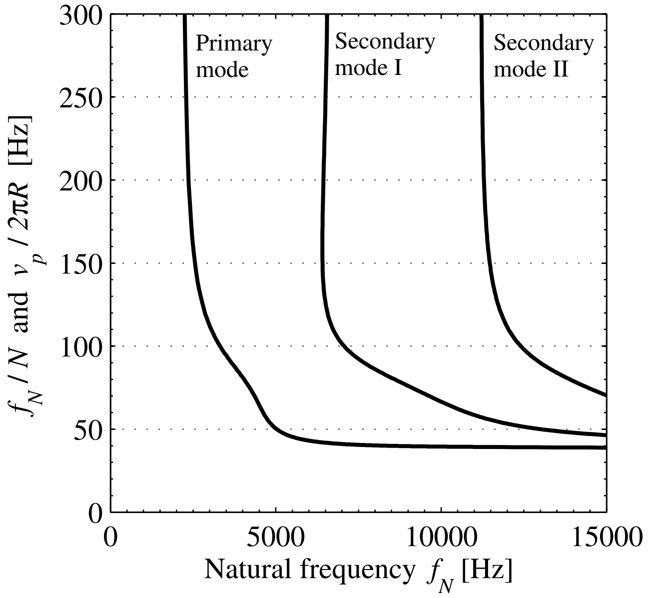

Figure 14: Natural frequencies divided by the principal mode number for the primary and secondary modes and equivalently the Rayleigh wave phase velocity according to Eq. (17) as a function of the natural frequency. Due to the vicinity of the discrete points, the curves are plotted as continuous lines.

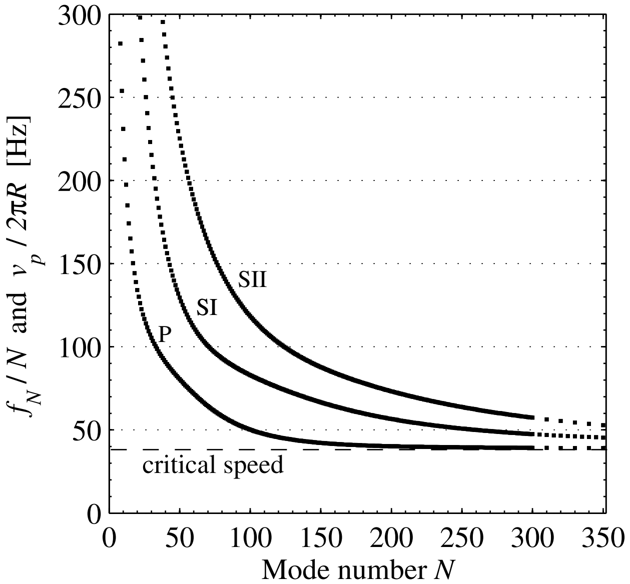

Figure 15: Natural frequencies divided by the principal mode number for the primary and secondary modes and equivalently the Rayleigh wave phase velocity according to Eq. (17) as a function of the principal mode number. Every mode up to $N = 350$ was calculated. From $N = 300$ to $N = 350$ only selected modes are shown.

also note the pioneering work of Goldstein, in which he showed that if the velocity of a semi-infinite uniform loading on an elastic half-space equals the velocity of the Rayleigh wave for the medium, a so-called Rayleigh wave resonance takes place [38]. When this happens, the Rayleigh waves arising at the front end of the load will have a common front, which moves together with the load. Thus, in the neighborhood of the front end of the load, a superposition of Rayleigh waves with the same phase occurs. As a result, the energy transmitted by the waves accumulates in the vicinity of the front end of the load.

Fig. 15 indicates that at the critical speed, a large number of primary modes should be active at the same time. According to Oden and Lin [12], in the case of a purely hyperelastic cylinder, there should exist infinitely many branches of solutions associated with the emergence of (tire) standing waves in the neighborhood of the critical speed. However, if there is viscoelasticity in the system, the response of the higher modes is effectively damped, or "washed out" [11]. It is worth noting in relation to the viscoelastic material model used in this work that the stiffness of the polymer begins to increase due to the transition from the rubber plateau towards the stiffer glass region of the polymer at high frequencies. Therefore, assuming that a wider relaxation spectrum would be used for the viscoelastic polymer, the mode family curves in Fig. 15 would start to increase at very high frequencies, leading to the conclusion that the number of active modes would be finite at the critical speed.

The natural frequencies and modes are affected by the thickness, density, and viscoelastic properties of the polymer cover. The effects of these parameters on the system, particularly on its critical speed, are of high interest considering practical applications. As an example, if the density of the polymer decreases, the natural frequencies increase and, thus, the critical speed increases. However, comprehensive material parameter variations are left out from this study due to the fact that they would mostly lead to quantitative changes in the dynamic behavior of the system, but not qualitative.

3.4. Traveling waves due to rolling contact

Fig. 16a shows the deformed shape of the polymer cover and the von Mises stress contour at the rotational frequency $f = 20$ Hz which is well below the critical speed, and Fig. 16b presents the corresponding contact pressure together with the radial and tangential displacements on the surface of the polymer cover in the nip area. The von Mises stress allows a brief inspection of the overall stress state and gives an indication of the location of a possible material failure. It can be seen, however, that the von Mises stresses are well below the yield stresses (~ 5 MPa) of the cover material in the studied case. In Fig. 16a, the stress maximum is located below the polymer cover surface near the midsurface. It is known from engineering practice that the temperature maximum in thin polymer covers is also located in the same manner, near the midsurface of the cover [39]. High von Mises stress concentrations can also be found on the bottom of the polymer cover due to high shear stresses. By a comparison between Figs. 16a and 6a, it is evident that in rolling contact the deformed shape of the cover is such that the primary mode family is the one being most powerfully excited at subcritical speeds. In Fig. 16b the maximum contact pressure, 0.22 MPa, is located practically at the center of the nip. The width of the nip is 10 mm. The radial displacement is almost symmetrical with respect to the center of the nip, with a slightly larger positive displacement bump at the leading edge, whereas the tangential displacement is nearly asymmetrical. The polymer cover response is quasi-static and local in the sense that no propagating waves are present.

Fig. 17 presents the radial displacement on the surface of the polymer cover in the nip area at the rotational frequency $f = 39.23$ Hz which has been computed by Eq. (6) according to the primary mode $N = 300$. This value is very near the critical speed. An incipient small amplitude traveling wave due to rolling contact can be seen at the trailing edge of the nip. In comparison to Fig. 16b the side bumps have also been increased. The wave moves together with the nip at the same speed. This behavior is analogous to that of a tire standing wave.

Figs. 18a and 18b present the radial displacement and the contact pressure in the nip area at the rotational frequencies $f = 50.16$ and 80.5 Hz, which have been chosen according to the primary modes $N = 100$ and 50, respectively, on the basis of Eq. (6). The corresponding deformed shapes of the polymer cover and the von Mises stresses are presented in Figs. 19a and 19b, respectively. At both rotational frequencies, a steady-state traveling wave due to rolling contact moving together with the nip at the same speed forms as in the case of $N = 300$ in Fig. 17. In Figs. 18a and 19a the primary eigenmodes can be

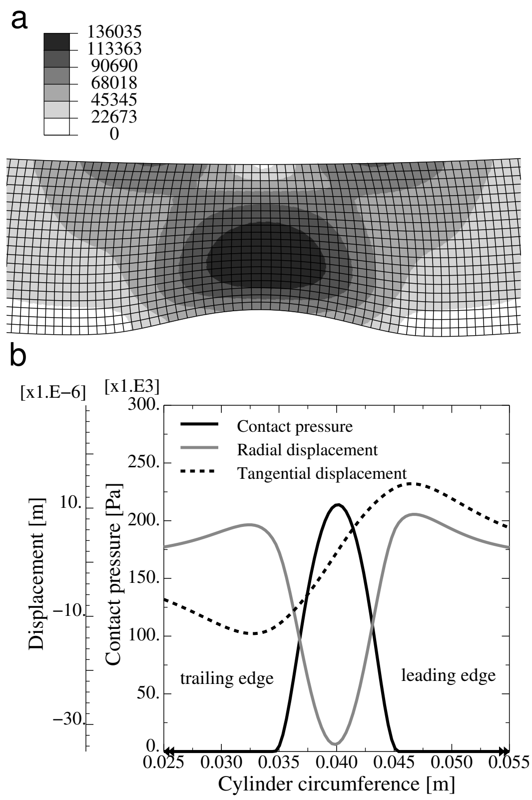

Figure 16: a) Deformed shape of the polymer cover in steady-state plotted with the von Mises stress contour [Pa] at the rotational frequency $f = 20$ Hz which is well below the critical speed. Displacements have been upscaled by a factor of 25. b) Contact pressure, and the radial and tangential displacements at the same instance on the surface of the polymer cover in the nip area.

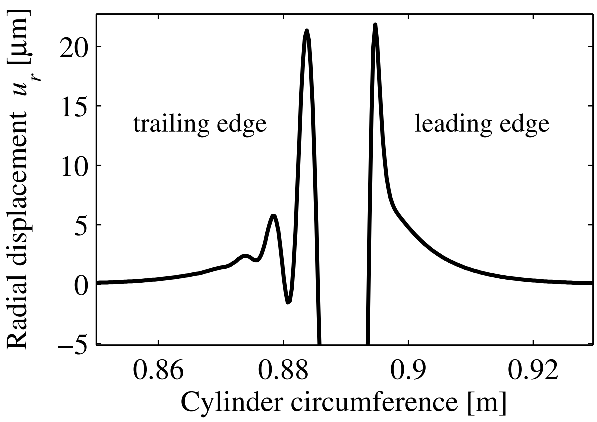

Figure 17: Radial displacement on the surface of the polymer cover in the nip area at the rotational frequency $f = 39.23$ Hz which has been chosen according to the resonance condition of the primary mode $N = 300$. An incipient traveling wave can be seen.

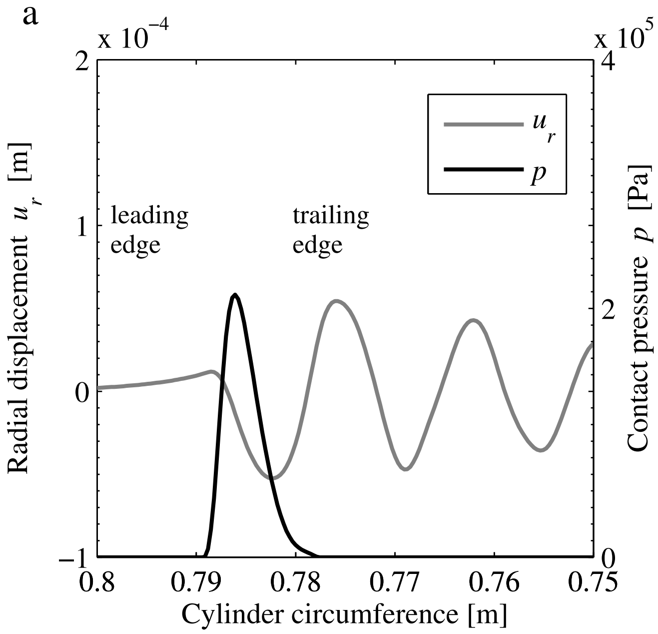

Figure 18: a) Radial displacement and the contact pressure on the surface of the polymer cover at the rotational frequency $f = 50.16$ Hz. The traveling wave due to rolling contact moving together with the nip starts to form at the leading edge of the nip. Note the shift of the pressure distribution towards the leading edge.

clearly seen to be dominant in the traveling wave, and the wavelength and the shape of the wave correspond approximately to those of the primary mode $N = 100$. At the higher rotational frequency $f = 80.5$ Hz in Figs. 18b and 19b, the traveling wave has a more irregular shape. The wave covers approximately one-half of the cylinder circumference, thus, from the eigenmode-based resonance point of view, the traveling wave phenomenon with the damping parameters and rotational frequencies used in this work does not appear to be a cumulative process that would increase the wave amplitude round by round. Note also that the traveling wave already starts to form at the leading edge of the nip, as has also been noted in [21]. It has been discussed on many occasions, whether the tire standing waves are perhaps created by the lift-off conditions at the trailing edge of the contact area. In the case of the studied numerical model, due to the fact that the wavy deformation already starts to form at the leading edge of the nip, it is clear that the traveling wave is not solely created by the lift-off conditions at the trailing edge of the nip (cf. Figs 16 and 18). Instead, the traveling wave behavior conforms perfectly to the Rayleigh wave resonance explanation given by Goldstein and described in detail in the previous section [38].

It can be seen in Figs. 18a and 18b that when the traveling wave is present, the nip "climbs up the hill", that is, it has moved towards the positive displacement bump at the leading edge in the same manner as the loading in the case of the elastic ring when the velocity of the load exceeds the minimum phase velocity of the waves in the ring [37]. This leads to a change in the contact pressure distribution so that it has a steeper slope at the leading edge and a higher maximum value, since the nip has penetrated deeper into the bump at the leading edge. It can be seen in Fig. 19 that the traveling waves bring about high stresses that spread along a considerable distance in the polymer cover. Furthermore, the waving leads to heat generation, which may hasten the structural failure of the polymer cover significantly. Actually, shock wave formations with reflections from the rigid bottom are clearly displayed, especially in Fig. 19b.

In both constant speed cases, that is, $f = 50.16$ and 80.5 Hz, a single surface node on the polymer cover is chosen and a frequency spectrum is calculated by the Fast Fourier Transform (FFT) from the radial displacement of the node after the nip has passed it and the node has oscillated freely outside the nip for a short time interval (~ 0.005 s) during which the waves have passed the node. For $f = 50.16$ Hz in Fig. 20,

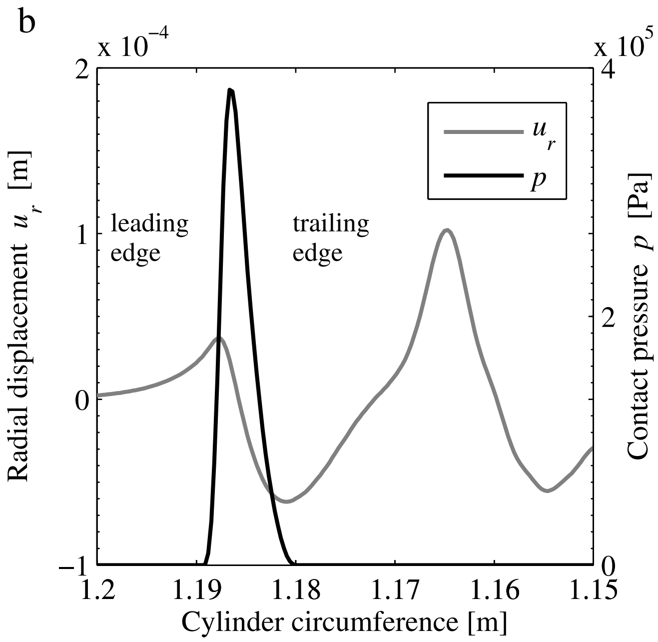

Figure 18: b) Radial displacement and the contact pressure on the surface of the polymer cover at the rotational frequency $f = 80.5$ Hz. Note the rise of the wave amplitude and pressure at the leading edge.

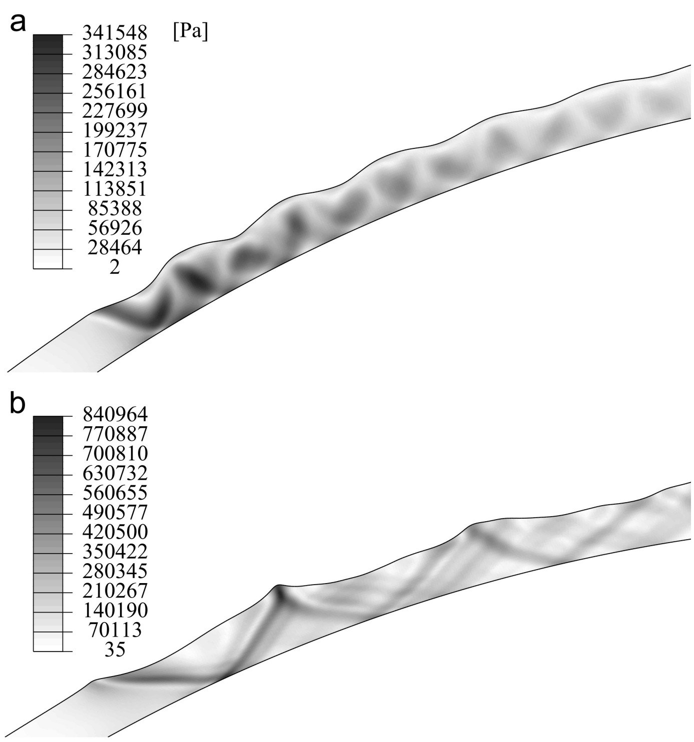

Figure 19: Deformed shape of the polymer cover with the von Mises stress contour [Pa] at the rotational frequencies a) $f = 50.16$ Hz and b) $f = 80.5$ Hz. The stresses are concentrated at the shock wave fronts.

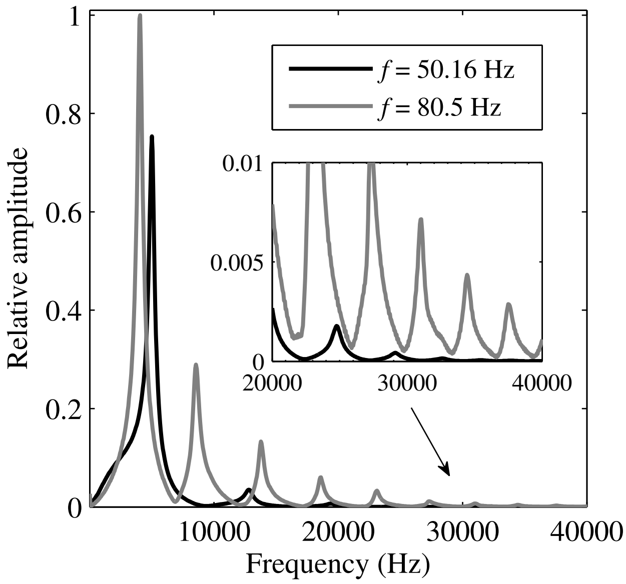

Figure 20: Frequency spectrum calculated by FFT from the radial displacement of a single surface node executing free oscillations for $f = 50.16$ and 80.5 Hz. The highest amplitude peaks are located at 5025 and 12830 Hz for $f = 50.16$ Hz and at 4030, 8555 and 13780 Hz for $f = 80.5$ Hz.

the frequency values of the two highest amplitude peaks coincide with the frequencies 5016 Hz ($N = 100$) and 12940 Hz ($N = 258$), read from Fig. 14 (Fig. 15) for the primary mode family and the secondary mode family I, with a relative error of less than 1 %. Similarly for $f = 80.5$ Hz, the three highest amplitude peaks are validated by Fig. 14 (Fig. 15), from which values 4025 Hz ($N = 50$), 8537 Hz ($N = 106$), and 13840 Hz ($N = 172$) can be read. It can be concluded that Fig. 20 gives the modal decomposition (without phase information) of the traveling waves, and the peaks correspond to the resonating modes according to Eq. (6) and Figs. 14 and 15. The amplitude peaks corresponding to the primary mode family are clearly the highest in Fig. 20. This is due to the fact that the nip deformation favors the primary modes.

It is also found, by additional numerical experimentation, that the contact pressure distribution or magnitude has no effect on the onset of the traveling wave phenomenon which is in accordance with the results of Padovan [10]. Larger contact forces, however, create traveling waves that are bigger amplitude-wise. Therefore, if the centrifugal forces acting on the polymer cover were accounted for, the extensional radial displacement would cause a slightly stronger traveling wave in the cover, while it would hardly affect the wave otherwise. As for the effect of the Coriolis force, the Coriolis acceleration can be approximated for a surface node (particle) by $a_C = 2\omega v_r$, where ω is the angular velocity and v_r the radial velocity of the node. Using the traveling wave case studied in Fig. 18a, it can be estimated that the magnitude of the Coriolis acceleration is typically only $1 - 3$ % of the total magnitude of nodal accelerations along the traveling wave at the trailing edge of the nip. We conclude that the Coriolis and centrifugal forces are of secondary interest with respect to the physical phenomena in the case of the present study.

The other amplitude peaks in Fig. 20 are related to the higher mode families. Therefore, Fig. 20 indicates that at high natural frequencies the higher mode family curves, if plotted in Fig. 14, would also approach the asymptotic and almost horizontal primary mode family curve of Fig. 14. Thus, for rotational frequencies approaching the critical speed $f = 39$ Hz, a large number of tightly packed modes fulfill or almost fulfill the resonance condition of Eq. (6) simultaneously. Therefore, a large number of eigenmodes resonate at the same time and it is difficult to see which are the dominant modes in the vicinity of the critical speed.

Each amplitude peak has a certain width in Fig. 20 which indicates that instead of a single natural mode from each family being active, a large number of modes are activated. This is a manifestation of the fact that a modified quasi-elastic Rayleigh wave corresponding to a certain mode family is a superposition of the modes in that family. These waves arising from the different mode families during the Rayleigh wave resonance combine into the wave which we refer to as *the traveling wave due to rolling contact*. Furthermore, due to the fact that a traveling wave in the polymer cover is composed of the eigenmodes of the cover, the critical speed which stems from the eigenmode analysis is also the minimum phase velocity of the traveling waves in the polymer cover, as already discussed in the previous section.

4. Conclusions

In this study, contact-induced traveling waves appearing at high rolling speeds on a viscoelastic cylinder cover in a two-cylinder rolling contact system were investigated using a two-dimensional plane strain finite element model. The characteristics of the traveling waves were studied through eigenmode analysis of the polymer cover and through dynamic analyses.

In the eigenmode analysis, it was found that an infinite number of different natural mode families exist for the polymer cover due to its finite thickness. A critical speed for the traveling wave phenomenon could be calculated on the basis of the eigenmode results for the rolling contact system. At the critical speed, a large number of eigenmodes satisfy the resonance condition practically simultaneously. At high rotational speeds the resonant speeds of the modes are more separated and fewer modes resonate simultaneously. Since the resonant speeds span a wide range, starting from the critical speed and extending to very high speeds, the traveling wave phenomenon can be described as an almost continuous resonance, where new resonating modes always enter into play when the rotating speed is increased. We conjecture that those eigenmodes which are supercritically excited give rise to a traveling wave behind the contact area due to the large phase lag between the excitation and response, while those excited subcritically with a small phase lag create a rapid quasi-static type response giving rise to a local deformation in front of and behind the contact area.

The traveling wave phenomenon was further elucidated in terms of wave propagation by performing dynamic rolling contact analyses. It was shown that at high rolling speeds traveling waves form on the polymer cover in the manner predicted by the eigenmode analysis. At the critical speed, there is, depending on the degree of viscosity in the system, little or no wave dispersion when the onset of the traveling wave phenomenon takes place as quasi-elastic modified Rayleigh waves start to arise at the front end of the contact area, the nip. The speed of the nip equals the minimum phase velocity of the modified Rayleigh waves and a conventional shock wave with a common front with the nip forms. Therefore, a superposition of waves with the same phase occurs and a traveling wave arises. The phenomenon is essentially a Rayleigh wave resonance. At higher speeds, there always exists modified Rayleigh waves with their phase velocity equal or very close to the velocity of the nip motion. Consequently, a shock wave is formed by these waves. Note, however, that modes that are excited subcritically are able to transmit deformation ahead of the contact area.

In conclusion, the conventional resonance point of view and the wave propagation aspect of the rolling contact-induced traveling wave phenomenon were found to be strongly interconnected. On closer inspection, traveling waves in the polymer cover were identified as superpositions of the primary and secondary eigenmodes of the polymer cover. It follows from this connection between the propagating wave and the eigenmodes that the appearance of *the traveling wave due to rolling contact* can be predicted by means of either eigenmode-based resonance considerations or the wave dispersion properties of the polymer cover. It was also found that in the case of the quasi-elastic Rayleigh waves, the value of the critical speed could be predicted to a good approximation by an equation for the Rayleigh wave phase velocity in an elastic half-space.

5. Acknowledgements

The financial support from the Ministry of Education and Culture of Finland through the Graduate School of Engineering Mechanics is gratefully acknowledged. CSC – IT Center for Science Ltd. is acknowledged for the allocation of computational resources.

References

[1] Johnson KL. Contact mechanics. Cambridge University Press; 1987.
[2] Kalker JJ. Three-dimensional elastic bodies in rolling contact. Kluwer Academic Publishers; 1990.
[3] Gonzalez JA, Abascal R. Efficient stress evaluation of stationary viscoelastic rolling contact problems using the boundary element method: Application to viscoelastic coatings. Eng Anal Bound Elem 2006;30(6):426-34.
[4] Sueoka A, Ryu T, Kondou T, Tsuda Y, Katayama K, Takasaki K, Yamaguchi M, Hirooka H. Polygonal deformation of roll-covering rubber. JSME Int J C-Dyn Con 1996;39(1):1-10.
[5] Yuan LH, Järvenpää V-M, Nonlinear vibrations in a covered roll system with viscoelastic contact, 2009;14(7):3170-78.
[6] Karttunen AT, von Hertzen R. Polymer cover induced self-excited vibrations of nipped rolls. J Sound Vib 2011;330(16):3959-72.
[7] Karttunen AT, von Hertzen R. On the self-excited vibrations of a viscoelastically covered cylinder in rolling contact using FE method. J Struct Mech 2011;44(3):231-42.
[8] Ames WF. Waves in tires. 1. Literature review on traveling waves. Text Res J 1970;40(6):498-507.
[9] Soedel W. On the dynamic response of rolling tires according to thin shell approximations. J Sound Vib 1975;41(2):233-46.
[10] Padovan J. Traveling waves vibrations and buckling of rotating anisotropic shells of revolution by finite elements. Int J Solids Structures 1975;11(12):1367-80.
[11] Padovan J. On viscoelasticity and standing waves in tires. Tire Sci Technol 1976;4(4):233-46.
[12] Oden JT, Lin TL. The general rolling-contact problem for finite deformations of a viscoelastic cylinder. Comput Method Appl M 1986;57(3):297-367.
[13] Padovan J, Paramadilok O. Transient and steady-state viscoelastic rolling-contact. Comput Struct 1985;20(1-3):545-53.
[14] Padovan J. Finite-element analysis of steady and transiently rolling nonlinear viscoelastic structure. 1. Theory. Comput Struct 1987;27(2):249-57.
[15] Kennedy R, Padovan J. Finite-element analysis of steady and transiently rolling nonlinear viscoelastic structure. 2. Shell and 3-dimensional simulations. Comput Struct 1987;27(2):259-73.
[16] Rabier PJ, Oden JT. Bifurcation in rotating bodies. Springer-Verlag; 1989.
[17] Krylov VV, Gilbert O. On the theory of standing waves in tyres at high vehicle speeds. J Sound Vib 2010;329(21):4398-408.
[18] Vinesse E, Nicollet H. Surface waves on the rotating tyre: An application of functional analysis. J Sound Vib 1988;126(1):85-96.
[19] Chatterjee A, Cusumano JP, Zolock JD. On contact-induced standing waves in rotating tyres: Experiment and theory. J Sound Vib 1999;227(5):1049-81.
[20] Perisse J. A study of radial vibrations of a rolling tyre for tyre-road noise characterisation. Mech Syst Signal Pr 2002;16(6):1043-58.
[21] Cho JR, Kim KW, Jeong HS. Numerical investigation of tire standing wave using 3-D patterned tire model. J Sound Vib 2007;305(4-5):795-807.
[22] Dassault Systemes Simulia Corp. Abaqus 6.10 Theory Manual. 2010.
[23] Simo JC, Hughes TJR. Computational inelasticity. Springer-Verlag; 1998.
[24] Ottosen NS, Ristinmaa M. The mechanics of constitutive modeling. Elsevier; 2005.
[25] Grimes RG, Lewis JG, Simon HD. A shifted block Lanczos-algorithm for solving sparse symmetric generalized eigenproblems. SIAM J Matrix Anal Appl 1994;15(1):228-72.
[26] Lessen M, Gangal DG. Effect of Coriolis acceleration on the vibrations of rotating disks. Appl Sci Res 1970;22(1):338-44.
[27] Huang SC, Soedel W. Effects of coriolis acceleration on the free and forced vibrations of rotating rings on elastic foundation. J Sound Vib 1987;115(2):253-74.
[28] Flanagan DP, Belytschko T. A uniform strain hexahedron and quadrilateral with orthogonal hourglass control. Int J Numer Meth Eng 1981;17(5):679-706.
[29] Belytschko T, Liu WK, Moran B. Nonlinear finite elements for continua and structures. Wiley; 2006.
[30] Soedel W. Vibrations of shells and plates. Marcel Dekker; 2004.
[31] Allard JF, Atalla N. Propagation of sound in porous media: Modelling sound absorbing materials. Wiley; 2009.
[32] Lowrie W. Fundamentals of geophysics. Cambridge University Press; 2007.
[33] Currie PK, O'Leary PM. Viscoelastic Rayleigh-waves. Q Appl Math 1977;35(1):35-53.
[34] Graff KF. Wave motion in elastic solids. Clarendon press; 1975
[35] Finnveden S. Waveguide finite elements for curved structures. J Sound Vib 2008;312(4-5):644-71.
[36] Kropp W, Sabiniarz P, Brick H, Beckenbauer T. On the sound radiation of a rolling tyre. J Sound Vib 2012;331(8):1789-1805.
[37] Metrikine AV, Tochilin MV. Steady-state vibrations of an elastic ring under a moving load. J Sound Vib 2000;232(3):511-24.
[38] Goldstein RV. Rayleigh waves and resonance phenomena in elastic bodies. PMM-J Appl Math Mec+ 1965;29(3):608-19.
[39] Chinn F. Dynamic instability of poly covered press rolls. Pulp Pap-Canada 1999;100(1):11-14.